JES Focus Issue of Selected Papers from IMLB 2018

Flexible S/DPAN/KB Nanofiber Composite as Binder-Free Cathodes for Li-S Batteries

Sandugash Kalybekkyzy,[1,2] Almagul Mentbayeva,[1,3] Memet Vezir Kahraman,[2] Yongguang Zhang,[3,4] and Zhumabay Bakenov[1,3,*,z]

[1]*National Laboratory Astana, Nazarbayev University, Astana 010000, Kazakhstan*
[2]*Department of Chemistry, Marmara University, Istanbul 34722, Turkey*
[3]*School of Engineering, Nazarbayev University, Institute of Batteries, Astana 010000, Kazakhstan*
[4]*School of Materials Science and Engineering, Research Institute for Energy Equipment Materials, Hebei University of Technology, Tianjin 300130, People's Republic of China*

Sulfur/dehydrogenated polyacrylonitrile/ketjen black (S/DPAN/KB) flexible nanofiber composite was prepared by electrospinning technique and tested as a freestanding cathode for high-performance flexible lithium/sulfur batteries. S/PAN/KB was dehydrogenated at 300°C without carbonizing and used as a cathode without any binder/current collector. The SEM observations of the obtained S/DPAN/KB nanofibers showed that the fiber diameters were in a range of 300–600 nm and the sample had a rough surface due to the presence of the S/KB particles. According to the SEM/EDS analysis sulfur is uniformly distributed within PAN fibers in both S/PAN/KB and S/DPAN/KB (heat treated) composites. The prepared binder-free S/DPAN/KB composite cathode exhibited a good electrochemical performance delivering a reversible capacity of 917 mAh g^{-1} after 150 cycles, exhibiting a coulombic efficiency about 100%, and demonstrating stable cyclability and good rate capability with a reversible capacity of 342 mA h g^{-1} at 1 C. The obtained composite cathode is highly flexible and can be used for LIB powering flexible electronic devices.
 [DOI: 10.1149/2.0571903jes]

Manuscript submitted November 5, 2018; revised manuscript received January 9, 2019. Published January 23, 2019. *This paper is part of the JES Focus Issue of Selected Papers from IMLB 2018.*

"Flexible electronic device" is a general term for devices that can operate when bent, folded, compressed, or stretched. Growing demand for such technologies stresses the importance of the characteristics like portability, convenience and design for consumer.[1] Nowadays, the market for flexible electronics is rapidly growing out of the boundaries of conventional electronics, and in the nearest future these technologies will be implemented to new areas like wearable electronics and medical devices.[1,2] Lithium-sulfur (Li/S) batteries are one of the most promising candidates of next-generation power sources for flexible devices.

Sulfur cathode has a theoretical specific energy of 2567 Wh kg^{-1}, which is remarkably higher than commercial $LiCoO_2$/C lithium-ion batteries.[3,4] Furthermore, sulfur-based cathodes have large capacity, safe operating voltage, and excellent potential for low cost production.[5] However, there are some issues that prevent the commercial application of Li/S batteries. The first major problem is insulating nature of sulfur, which results in poor electrochemical accessibility and low utilization of sulfur in the electrode. The second issue is a high solubility of the electrochemical reaction products, the lithium polysulfides, in organic liquid electrolytes, and the third is a large volume variation of sulfur during cycling. All these problems result in a rapid capacity fading, low coulombic efficiency, decrease in power capability and poor cycling stability.[6,7] Various strategies have been developed to solve the above-mentioned problems, such as encapsulation of sulfur in nanostructured carbon materials and combining it with conductive polymers like polyacrylonitrile,[7,8] polyaniline,[9,10] polythiophene.[11] Also, loading elemental sulfur into different porous materials like mesohollow, microporous carbon fibers is another established option.[12,13]

One of the main approaches to make sulfur/carbon (S/C) composites electrochemically active is preparing a composite cathode by loading sulfur into nanopores of conductive carbon matrices. However, the shuttling of polysulfides leading to the capacity fading still remains unsolved problem for such composites.[14] It should be noted that conventional S/C composite electrode materials need large amount of conductive additives and polymer binders to provide mechanical stability and electrical connectivity to the whole system. The addition of conductive additives and binders during preparation of the electrode material decreases the sulfur content, which distinctively decreases the overall energy density of battery.[15] Considering these drawbacks an effective way to assemble sulfur batteries with high volumetric energy and power density is to develop a binder-free, freestanding and flexible electrode.[16] Such systems could be very attractive because all the components could participate in lithium storage.

In our previous works flexible S/PAN/C composite materials were demonstrated as freestanding high performance cathodes for Li-S battery.[17,18] Zeng et al. reported sulfur embedded microporous carbon nanofibers as flexible freestanding cathodes for Li-S batteries.[6] Nanofibrous structure garners increasing attention in the synthesis of flexible materials for Li-ion batteries.[19] They have large surface area, high length/diameter ratio, good flexibility, high porosity and multiple functionalities.[20] One of the simplest methods to prepare nanofibers is the electrospinning technique which can be applied to different types of polymers, polymer alloys, and polymers/inorganic composite materials.[21–23] The fibers synthesized by electrospinning are flexible in choosing the components, in morphology, structure and functionality, so they can be widely applied in LIBs.[24,25]

The major problems in S/PAN nanofiber cathode materials are low electrical conductivity and low sulfur content.[26,27] As the result of these drawbacks an electrode is commonly prepared by coating the slurry of obtained S/PAN nanofibers, conductive additives and binders on a current collector.[14,28,29] However, as mentioned above the addition of binders decreases the sulfur content in the electrode. In order to increase sulfur mass loading, there were a number of studies reporting binder free, freestanding sulfur-based nanofiber cathodes with carbonized PAN at high temperature (above 700°C).[6,30,31]

In our work we prepared the PAN nanofibers filled with S/KB particles (denoted as S/PAN/KB, where KB is Ketjen Black) by a single nozzle electrospinning technique. Further S/PAN/KB nanofibers were heated at 300°C temperature to make PAN dehydrogenated, sulfurized, and, therefore, conductive. Benefitting from its structural features, the as-prepared S/DPAN/KB nanofiber cathode exhibited good compatibility with the conventional carbonate-based electrolytes and showed a high coulombic efficiency, long cycle life

*Electrochemical Society Member.
[z]E-mail: zbakenov@nu.edu.kz

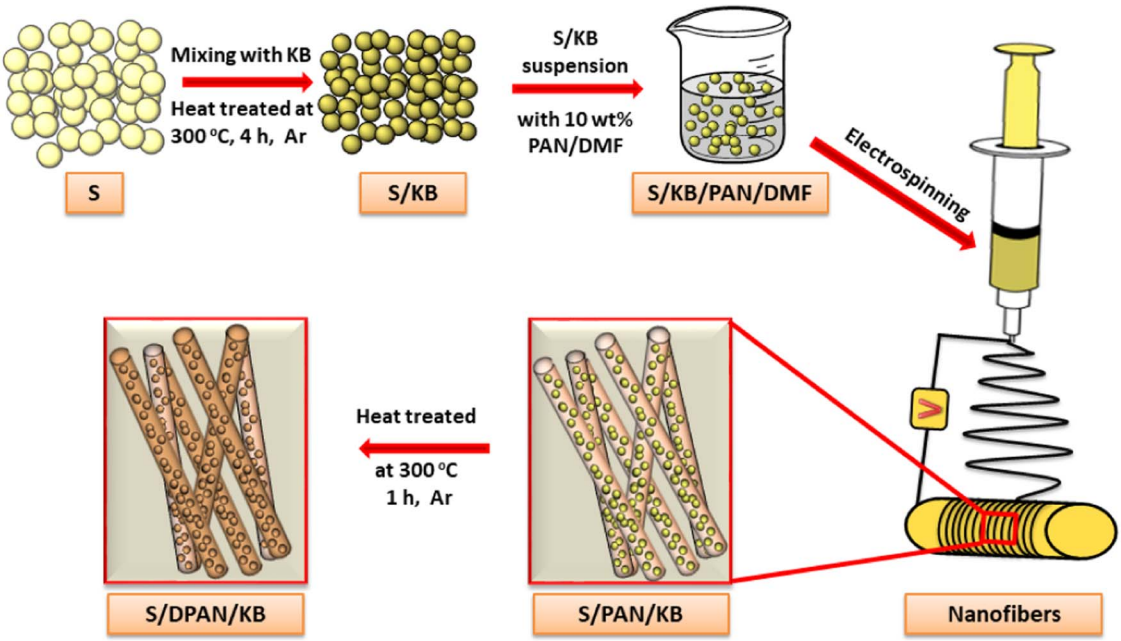

Figure 1. Schematic illustration of electrospinning process and fabrication of flexible S/DPAN/KB composite cathode.

and good rate capability, demonstrating a great prospect for battery applications.

Experimental

Materials.—Polyacrylonitrile (average M_w = 150,000, J&K Scientific), sulfur (98%, GOST 127.1, Tengizchevroil, Kazakhstan), Ketjen Black (MTI Co., 99.5% purity), N,N-Dimethylformamide (DMF, 99%, Sigma-Aldrich), polyvinylidene fluoride (PVdF, Kynar, HSV900), N-methyl-2-pyrrolidone (NMP, Sigma-Aldrich, 99.5% purity) were used as received without further purification.

S/KB composite preparation.—KB was used as conducting matrix to prepare S/KB composite. S/KB composite was prepared by mixing sulfur and KB in a weight ratio of 95:5, and heat treating in a tubular furnace (Across International, STF1200) at 300°C in argon for 4 h. After cooling down, the resulting sulfur impregnated KB composite was ground by ball milling (Fritsch, Pulverisette 7) for 4 h at 600 rpm. The ball milled composite was used further to prepare the spinning solution.

Fabrication of S/PAN/KB nanofiber composite electrode by electrospinning.—Schematic illustration of the electrospinning process is shown in Figure 1. The spinning solution was prepared by dissolving 1 g of PAN in 9 g DMF and continuous overnight stirring. S/KB composite was homogeneously dispersed in the PAN solution by sonication for 5 h. Optimized weight ratio of PAN, S/KB composite was 2:3. Dispersed solution was loaded into 10 ml syringe with a stainless steel nozzle and spun by applying voltage of 17 kV with a solution flow rate of 1 mL h^{-1} (Inovenso, Ne200). The distance between rotating cylinder and nozzle tip was kept as 12 cm. Nanofibers were collected onto a carbon coated aluminum foil (MTI Co.). The obtained S/PAN/KB composite nanofibers were heated in a tubular furnace in Ar with a heating rate of 10°C min^{-1} to 300°C and kept at this temperature for 1 h to cyclize PAN polymer chains and sulfurize dehydrogenated PAN in the S/KB composite.[32,33] The resulting S/DPAN/KB nanofiber composite was freestanding, flexible and was directly used as an electrode without any binder.

Structure Characterization

The morphologies of the samples were characterized by Filed-Emission Scanning electron microscopy (FESEM, JEOL JSM-7500F), energy-dispersive spectroscopy (SEM/EDS, Hitachi, TM3030). X-ray diffraction (XRD, Rigaku SmartLab), X-ray photoelectron spectroscopy (XPS, Thermo MultiLab 2000) and Fourier-transform infrared spectroscopy (FTIR, Agilent Technologies, Cary 600) were used to characterize the structural properties of the samples. The sulfur content was determined using chemical analysis (CHNS, Vario Micro Cube, Elementar).

Electrochemical measurements.—All the electrochemical tests were carried out in an argon filled glove box (MasterLab, MBraun) using coin-type cells (CR2032), with lithium metal discs as both negative and reference electrode, polypropylene membrane as a separator (Celgrad 2400) and a liquid electrolyte $LiPF_6$ in ethylene carbonate/dimethyl carbonate/diethylene carbonate (EC:DMC:DEC, volume ratio of 1:1:1, Targray). The prepared S/DPAN/KB nanofiber composite was cut into disks of 1 cm in diameter and used as a freestanding cathode to assemble the cells. The cells were galvanostatically cycled at different current densities in a potential range of 1.0–3.0 V vs. Li/Li^+ on multichannel battery tester (BT-2000, Arbin Instruments Inc.). Specific capacity and current density were calculated based on the weight of sulfur in the electrode. Cyclic voltammetry (CV) was conducted over a potential range from 1 to 3 V vs. Li/Li^+ at a scan rate of 0.1 mV s^{-1} (VMP-3 potentiostat/galvanostat, Bio-Logic Instruments). All the electrochemical measurements were carried out at room temperature. For comparison, a conventional S/DPAN/KB cathode on Al foil current collector was also prepared and tested under similar conditions. In this case, 80 wt% of S/DPAN composite, 10 wt% KB and 10 wt% polyvinylidene fluoride (PVdF) were dispersed in NMP. The resulting slurry was applied onto Al foil using doctor blade technique and vacuum dried at 60°C for 12 h. In addition, S/KB composition was prepared with the same method in order to compare with S/DPAN systems. Specific capacity and current density were calculated based on the weight of sulfur in the electrode. The mass loading of sulfur was around 1.5 mg cm^{-2} for all samples. In all experiments the area of the cathode was 1.76 cm^2. For bending test the pouch-type cell was assembled in the argon filled glove box with one layer of Li metal anode and two layers freestanding

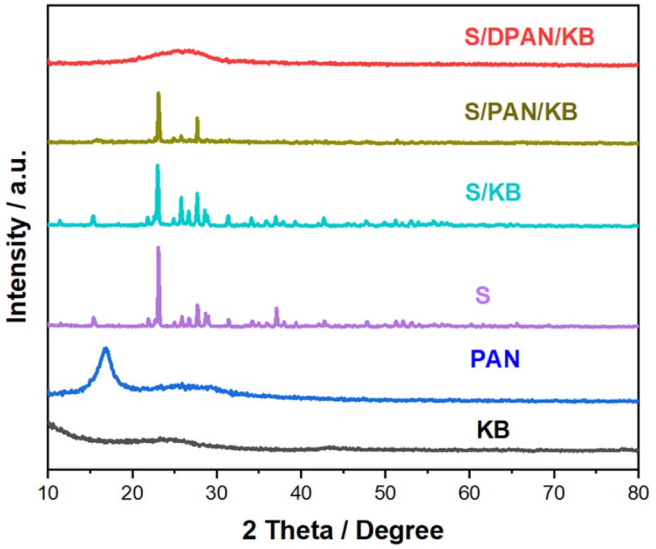

Figure 2. XRD patterns of KB, PAN, sulfur, S/KB, S/PAN/KB and S/DPAN/KB composite nanofibers.

S/DPAN/KB nanofiber composite cathode with dimensions of 25 × 30 mm separated by porous polypropylene membrane.

Results and Discussion

Flexible freestanding S/DPAN/KB cathode for lithium-ion sulfur batteries was prepared by electrospinning technique. The maximum content of sulfur allowed to prepare and maintain stable and flexible S/PAN/KB nanofibers was 54 wt%. In order to achieve 54 wt% S content, PAN and S/KB composite ratio in the solution was varied. It was found that the optimal weight ratio of PAN to S/KB in the spinning solution is 2:3. After the heat-treatment of S/PAN/KB nanofibers at 300°C for 1 h, the content of sulfur in the composite decreased to 30 wt% due to the sublimation of sulfur. The sulfur content was determined using a CHNS analyzer which is presented in Table S1. The partially pyrolyzed and cyclized conductive PAN stabilizes sulfur and suppresses its dissolution into electrolyte.[32,34] The phase composition of the S/KB, S/PAN/KB and S/DPAN/KB composites was studied using X-ray diffraction (XRD). The XRD patterns of these composites are shown in Figure 2 along with the patterns of the starting S, KB and PAN components. One can see that KB shows a characteristic diffraction peaks with low intensities between 20 and 27 2θ while pristine S exhibits sharp and intense diffraction peaks between 10 and 60 2θ, which indicates its crystalline state. A strong peak at the 2θ = 16.9 observed in the XRD pattern of PAN is due to its crystallinity as well. In the case of the S/KB composite and S/PAN/KB nanofibers, the peaks of crystalline S are still visible but their intensities are substantially reduced due to the uniform distribution of sulfur in the KB and PAN. The characteristic peaks of crystalline sulfur were not observed after heat-treatment of the S/PAN/KB nanofibers in which the content of sulfur was 30 wt%. It indicates that sulfur is amorphous and homogeneously distributed in the S/DPAN/KB matrix and could be bound with dehydrogenated PAN during the heat-treatment as mentioned in our previous reports.[17] Also, Myung et al. proposed that carbon-sulfur chemical bond exists in S/DPAN composites as the interface between sulfur particle and the DPAN layer which explains the reason for the good electrochemical performances of the S/DPAN/C composites.[35] The FTIR spectra also support a suggestion of formation of heterocyclic compound in the process of dehydrogenation of PAN with sulfur (Figure 3). In the FTIR spectrum of PAN shown in Figure 3 the peaks at 2244 cm^{-1} and 1454 cm^{-1} represent the –CN and $–CH_2$ groups, respectively. In the obtained composite S/DPAN/KB these characteristic peaks disappear and a new peak appears at 1494 cm^{-1}, which corresponds to a C=C double bond, and a peak at 1358 cm^{-1}

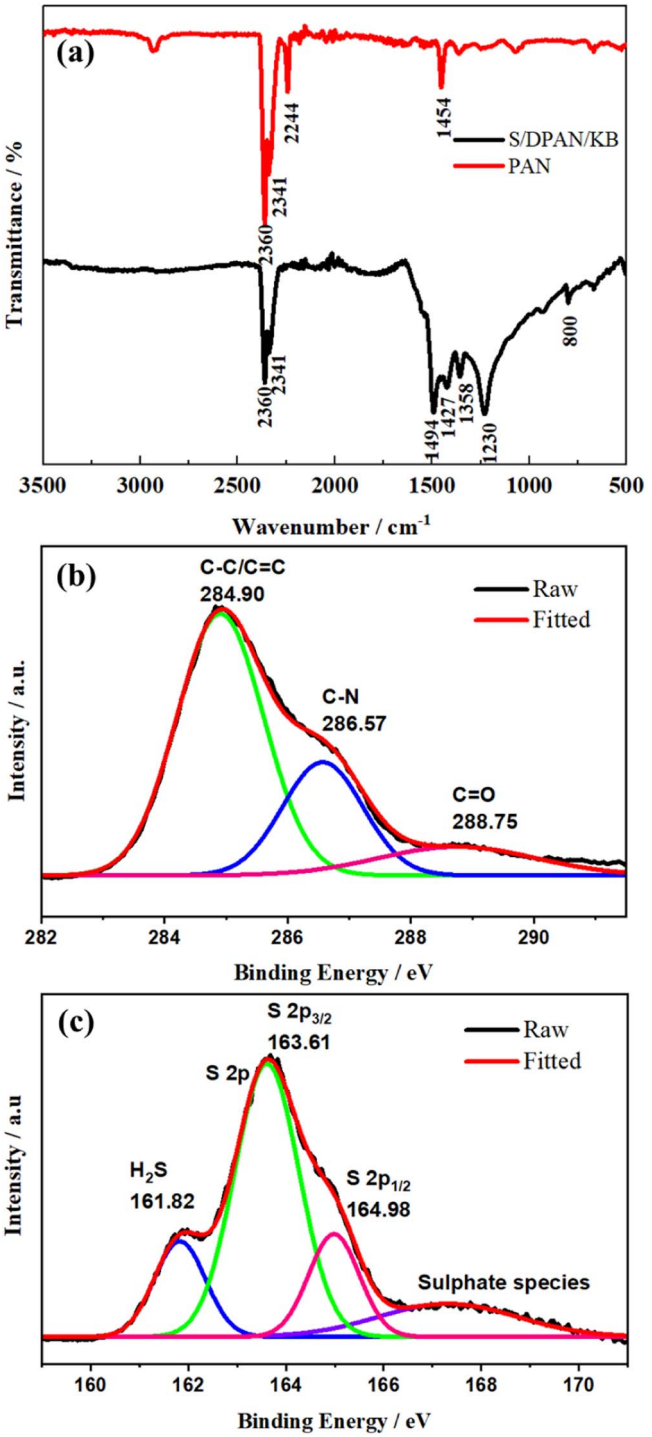

Figure 3. (a) FTIR spectra of PAN and S/DPAN/KB; XPS analysis of S/DPAN/KB nanofibers (b) C 1s spectrum; (c) S 2p spectrum.

is due to a –CH deformation. The peaks at 1427 cm^{-1} and 800 cm^{-1} indicate the formation of cyclic structure during the heat-treatment of S/PAN/KB. As reported by J. Wang et al., during heating process sulfur dehydrogenates PAN, which results in forming a conductive chain and the –CN functional groups cyclize in the melt state, resulting in a thermally stable heterocyclic compound, in which elemental sulfur is embedded.[34]

X-ray photoelectron spectroscopy (XPS) was used to characterize the chemical composition of the S/DPAN/KB nanofibers. Figure 3b shows the XPS spectra in the C 1s region. Fitted curves reveal that

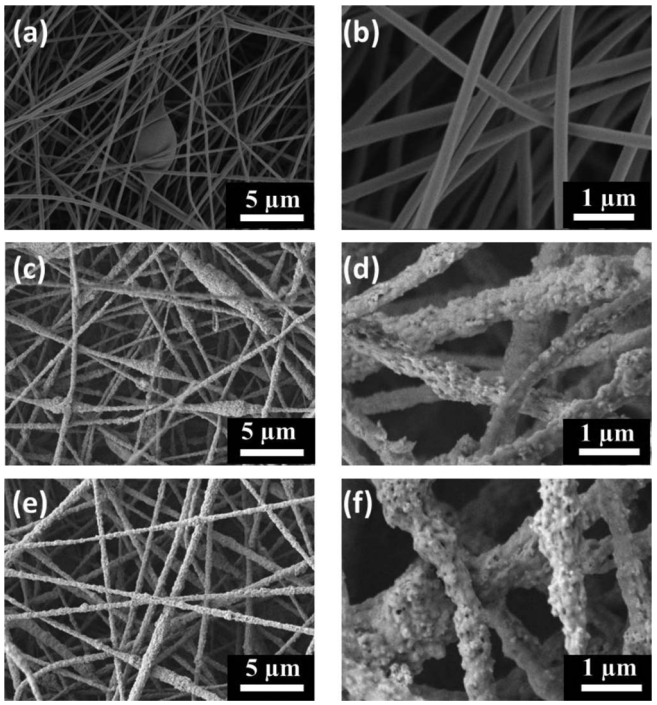

Figure 4. SEM images of (a, b) PAN, (c, d) S/PAN/KB nanofibers and (e, f) S/DPAN/KB freestanding composite cathodes.

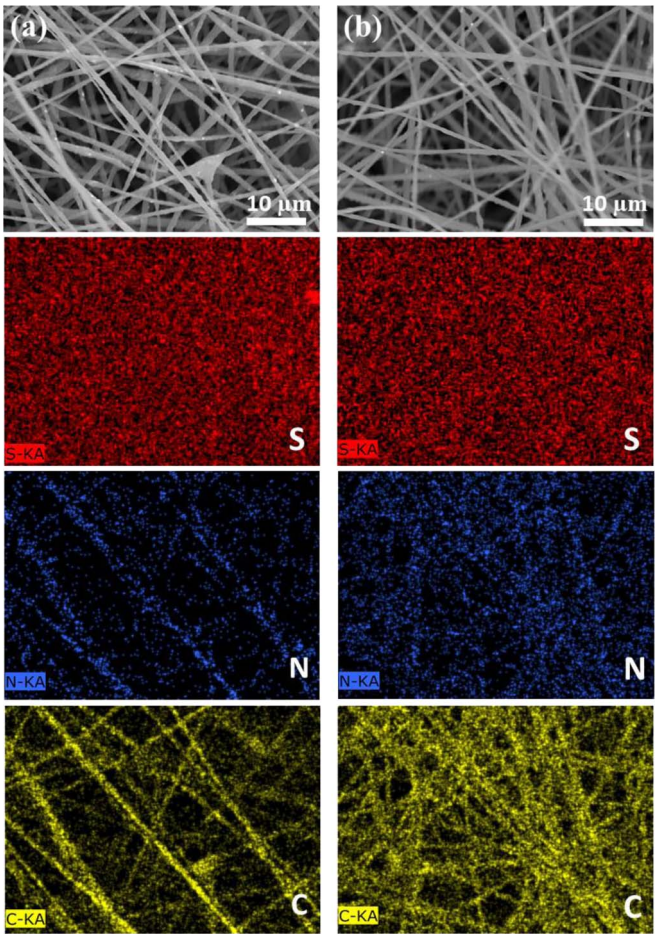

Figure 5. SEM/EDS mapping showing the distribution of sulfur (S), nitrogen (N) and carbon (C) in the composites (a) S/PAN/KB with 54 wt% sulfur and (b) S/DPAN/KB with 30 wt% sulfur.

the C 1s band can be split into three peaks. The main peak at 284.90 eV corresponds to the sp^2-hybridized carbon, the peak at 286.57 eV corresponds to the C–N bonds, and partially to the C–S weak bond as well.[14] The peak at 288.75 eV can be attributed to the C–O species formed by carbon oxidation during the heating process. For the S 2p spectrum (Figures 3c), the peaks at 164.98 eV and 163.61 eV are assigned to S 2p 1/2 and S 2p 3/2 spin-orbit levels of elemental sulfur. The lower binding energy of the S 2p 3/2 state (163.61 eV) than that of elemental sulfur (164.0 eV) indicates the presence of the weak C–S bond in the nanofibers. The minor peak centered at 167.31 eV arises from the sulfate species formed by the oxidation of elemental sulfur during the preparation process. The peak at 161.82 eV can be attributed to the adsorbed H_2S by-product generated in the cyclization reaction of S/DPAN/KB nanofibers.

The morphology of the as-prepared S/DPAN/KB fibers was investigated using SEM. As observed in the SEM images of both S/PAN/KB and S/DPAN/KB, the obtained fibers have the diameter ranging from 300 to 600 nm, and own a similar morphology and a rough surface due to the presence of S/KB particles (Figures 4c–4f). The fiber diameters are smaller and have no pores only in the case of PAN nanofibers (Figures 4a–4b), and this difference with the S/PAN/KB composite was also attributed to the addition of S/KB. Along with this, it shows perceptible pores on the surface of the S/DPAN/KB composite nanofibers which are related with the sublimation of sulfur during the heat-treatment and dehydrogenation of PAN, which lead to the formation of these pores and a large weight loss. The uniform distribution of components in the fibers was confirmed by SEM/EDS elements mapping in the obtained composites (Figure 5). As shown in the first column of Figure 5a, the mapping of sulfur, carbon and nitrogen in the composite indicates that sulfur is uniformly distributed within the PAN fibers, and the S/KB composite was homogeneously mixed before adding to the spinning solution. After the dehydrogenation of the S/PAN/KB composite the S content decreased as explained above, and due to this phenomenon the carbon and nitrogen distribution can be seen more clearly in the SEM/EDS data in the case of S/DPAN/KB (Figure 5b).

The specific surface area analysis was performed by nitrogen Brunauer-Emmett-Teller (BET) adsorption measurements and Barrett–Joyner–Halenda (BJH) pore size and volume analysis. Figure 6a shows the N_2 sorption/desorption isotherms and Figure 6b presents the pore-size distribution curves of PAN, S/PAN/KB and S/DPAN/KB. S/PAN/KB and S/DPAN/KB exhibit hysteresis curves over a broader range of P/P_0 (0.4–0.9), which is a general characteristic of a mesoporous material. On the other hand, PAN shows a typical type II isotherm which is generally observed in nonporous materials.[36] The BET surface area of PAN obtained by N_2 adsorption analysis is low, 1.26 $m^2\ g^{-1}$. In the case of S/PAN/KB and S/DPAN/KB, the surface areas are around 21.39 $m^2\ g^{-1}$ and 94.73 $m^2\ g^{-1}$, the BJH mean pore diameters are 3.711 nm and 3.717 nm, respectively. After the heat-treatment of S/PAN/KB nanofibers, the BET surface area increased due to dehydrogenation of PAN and sublimation of sulfur. The porous structure of the S/DPAN/KB composites can help to avoid the dissolution of polysulfides which is one of the main issues of sulfur-based cathode. It improves the capacity retention by hindering the shuttle effect.

The electrochemical performance of the prepared S/DPAN/KB nanofibers as freestanding cathodes for Li-S batteries were examined in lithium half-cells and compared with the performance of the S/KB and S/DPAN/KB electrodes prepared by slurry casting on Al foil with addition of conductive agent and binder. Figure 7 shows the first two CV curves of a cell with (a) S/KB and (b) S/DPAN/KB electrodes on Al foil, and (c) a freestanding nanofiber composite S/DPAN/KB cathode cycled in a potential range of 1.00 – 3.00 V at a scan rate of 0.1 mV s^{-1}. As shown in Figure 7a, the S/KB composite cathode shows two cathodic peaks corresponding to the typical for the S/C composite cathodes two-step conversion reactions. The peak centered at 2.2 V corresponds to the transformation of S_8 to Li_2S_n ($4 \leq n <$

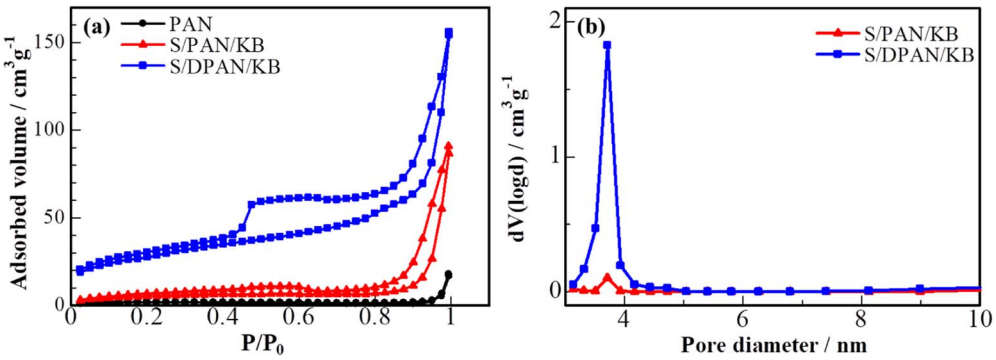

Figure 6. (a) N_2 sorption/desorption isotherms of PAN, S/PAN/KB and S/DPAN/KB and (b) pore-size distributions curve of S/PAN/KB and S/DPAN/KB.

8), while the other peaks centered around 1.8 V correspond to the further reduction of Li_2S_n ($4 \leq n < 8$) to Li_2S/Li_2S_2.[6] There are two partially overlapping anodic peaks in case of the S/KB composite. The main one is centered at ca. 2.9 V (vs. Li/Li^+), and the minor one is centered at a slightly lower potential of 2.7 V, which corresponds to the conversions of Li_2S/Li_2S_2 to the low-order polysulfides and the low-order polysulfides to high-order polysulfides, respectively. In the case of S/PAN cathode, CV curves are different from that of the S/KB composite. One can observe a broad reduction peak at around 1.6 V vs. Li/Li^+ in the first CV cycle of the conventionally prepared S/DPAN/KB composite, which shifts to the higher potentials upon the following cycle (Figure 7b). The further cycling shows two overlapping and reversible reduction peaks at around 2.0 and 1.7 V and a broad oxidation peak at around 2.5 V. Also, there is the first small reduction peak at 2.0 V related to the formation of polysulfides and the second one at 1.7 V related to the further reduction of the polysulfides into lithium sulfide.

Figure 8a shows the charge-discharge profiles of the S/DPAN/KB electrode at 0.1 C, which exhibits a large initial discharge capacity of 1759 mA h g^{-1}. The composite cathode delivers within the second cycle a high discharge capacity of 1128 mAh g^{-1} and a high coulombic efficiency up to ~99%, which corresponds to areal capacity of 1.70 mA h cm^2, since the mass loading of S was around 1.5 mg cm^{-2}. Figure 8b shows that the cell exhibits stable cycling performance at least for 150 cycles and maintaining a reversible capacity of 917 mAh g^{-1} after 150 cycles. The value of capacity fading per cycle is as small as 0.017%. Along with this, the S/DPAN/KB composite cathode exhibits a high coulombic efficiency about 100% over cycling, which could be due to the suppression of the polysulfides shuttle effect by the molecular level binding of sulfur with DPAN and also by porous structure of the fibers, which effectively store soluble products of the reduction of sulfur.

For comparison, the cyclability and rate performance of the S/KB and S/DPAN/KB electrodes prepared by slurry casting on Al foil with addition of conductive agent and binder were analyzed (Figure S1). Sulfur content in the composites was around 40 wt% and mass loading of sulfur was kept around 1.5 mg cm^2. Freestanding S/DPAN/KB nanofiber composite cathode and the one prepared by slurry casting show very similar cyclability and gravimetric capacity based on mass of sulfur. However, freestanding S/DPAN/KB composite cathode has 340 mA h g^{-1} capacity calculated based on the composite electrode weight. It is higher for 20% then the capacity of S/DPAN/KB electrodes prepared by slurry casting on Al foil with addition of conductive agent and binder, which is 280 mA h g^{-1}, calculated for the electrode mass including the weight of current collector with the similar sulfur loading of 1.5 mg cm^{-2}. At the same time the cell with S/KB electrode perform poor cyclability and low coulombic efficiency (~80%) due to the dissolution of polysulfide and so called shuttle effect.

In addition to a high capacity and good cyclability, the S/DPAN/KB nanofiber cathode without any current collector and conductive additives demonstrates a good rate capability as well. As shown in Figure 8c, the nanofiber electrode delivers a discharge capacity of 1148 mA h g^{-1} at 0.1 C, 977 mA h g^{-1} at 0.2 C, 483 mA h g^{-1} at 0.5 C, and 342 mA h g^{-1} at 1 C. S/KB and S/DPAN/KB electrodes prepared by slurry casting on Al foil (Figure S1 c and d) exhibit slightly better C rate performance compared with freestanding electrode, delivering discharge capacity around 400 and 700 mA h g^{-1} at 1 C, correspondingly. The difference in capacity of cathodes with and without current collector increases with the higher current density, which is related to the rise of resistance in case of freestanding electrode. Nevertheless, the freestanding electrode can still deliver a considerably high reversible capacity of 342 mA h g^{-1} even at a current density of 1 C. Once the current density is reduced back to 0.1 C at the end of the rate capability tests, the discharge capacity of the electrode recovers to 1020 mA h g^{-1}, showing a good tolerance toward a high electric current impact.

After cycling for 100 cycles at current of 150 mA g^{-1}, the cell was disassembled in the fully charged condition and the morphology of the post-cycled freestanding S/DPAN/KB nanofiber cathode was observed. As shown in Figure S2 the shape, size and structural integrity of the original nanofiber electrode are well maintained, demonstrating good structural stability. S/DPAN/KB composite cathode retains the

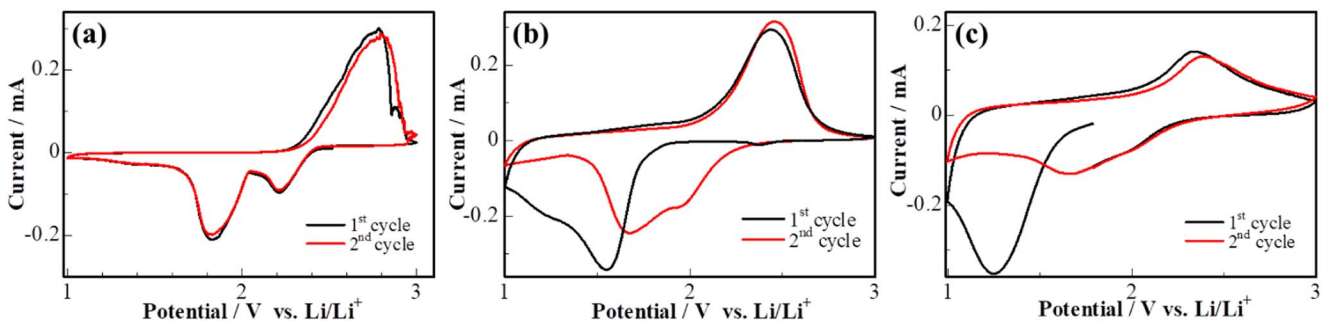

Figure 7. CV profiles of cells (a) with S/KB, (b) conventional S/PAN/KB composite and (c) freestanding S/DPAN/KB nanofiber cathodes. Scan rate 0.1 mV s^{-1}.

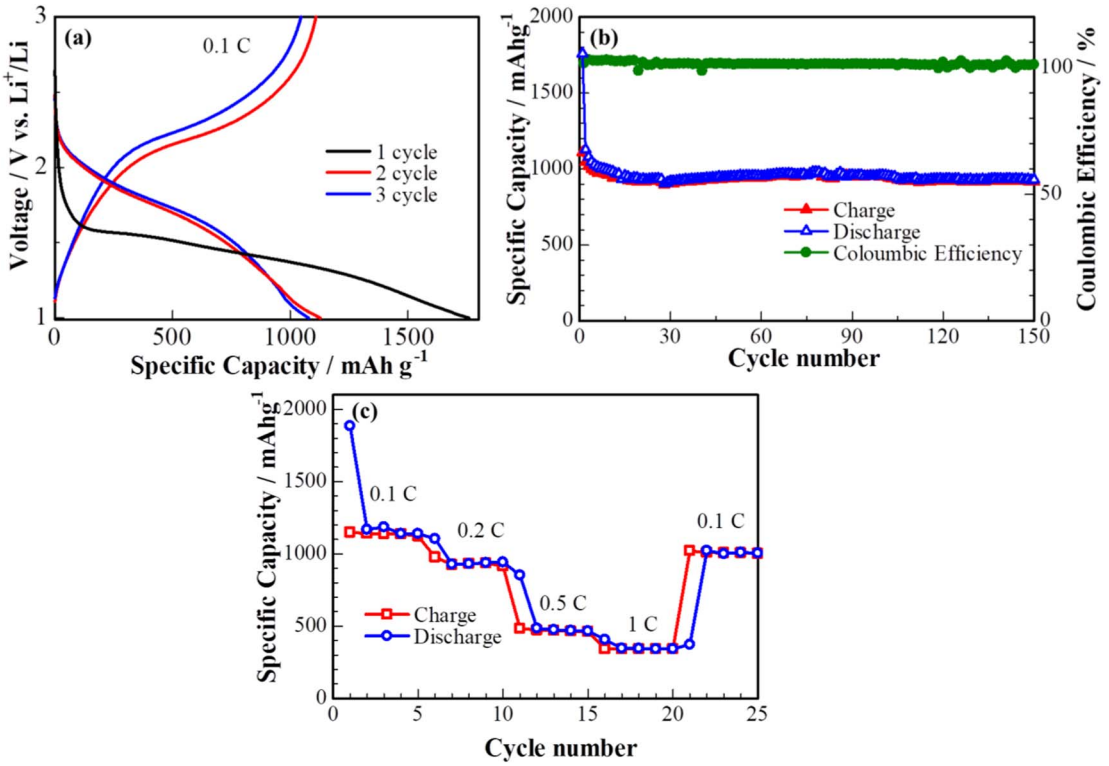

Figure 8. (a) Potential profiles, (b) cycle performance at 0.1 C, and (c) and rate capability of cells with freestanding S/DPAN/KB composite cathode nanofibers.

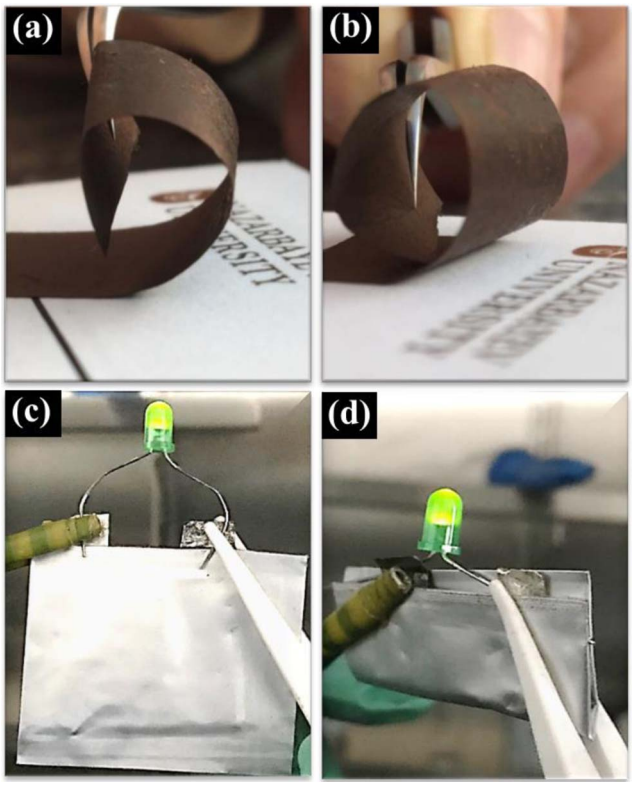

Figure 9. Photographs showing (a, b) the freestanding flexible S/DPAN/KB nanofiber composite cathode and (c) illustration of pouch cell with S/DPAN/KB nanofiber composite cathode powering LED lamps under normal static condition and (d) under being manually bent.

diameter of fibers with no significant change. The surface morphology becomes rougher compared to the fresh electrode, but there is no significant change in the BJH mean pore diameter and surface area of post-cycled nanofiber cathode as shown in Figure S3. The surface area of S/DPAN/KB after 100 cycles is around 91.28 $m^2\ g^{-1}$ and BJH mean pore diameter is 3.9365 nm.

Since the S/DPAN/KB nanofiber composite is flexible, the pouch-type cell based on them can be flexible and bendable as well, as shown in Figure 9 and Figure S4. Even after folding several times, the battery can still power light-emitting diodes (LEDs) without noticeable dimming.

Conclusions

In summary, we have successfully prepared a sulfur-PAN nanofiber-ketjen black freestanding composite cathode for flexible Li-S batteries by electrospinning technique. Optimal conditions of spinning process were established for preparation of S/PAN/KB nanofibers with a high sulfur content. Electrochemically active S/DPAN/KB cathode was prepared by heating at low temperature without carbonization of PAN to insure the flexibility and stability of this binder-free cathode. When used as cathode for Li-S batteries, S/DPAN/KB exhibits a good electrochemical performance in carbonate-based electrolyte. It exhibits stable cycling performance at least for 150 cycles and maintains a reversible capacity of 917 mAh g^{-1} after 150 cycles and a good rate capability with a reversible capacity of 342 mA h g^{-1} at 1 C. The value of capacity fading per cycle is as small as 0.017%. Within these properties, the highly flexible composite cathode can be produced in bigger sizes by electrospinning technique and used for LIB powering flexible electronic devices.

Acknowledgments

This research was supported by the targeted state program No. BR05236524 "Innovative Materials and Systems for Energy Conversion and Storage" from the Ministry of Education and Science of the

Republic of Kazakhstan for 2018–2020 and by the Social Policy grant "Preparation of flexible electrodes and electrolytes" from Nazarbayev University. The authors wish to express their sincere thanks to Professor Sung-Soo Kim and Nurzhan Umirov from Chungnam National University for generous help with performing XPS analysis and comments that greatly improved the manuscript.

ORCID

Almagul Mentbayeva https://orcid.org/0000-0001-9132-1173
Zhumabay Bakenov https://orcid.org/0000-0003-2781-4955

References

1. H. Gwon, J. Hong, H. Kim, D.-H. Seo, S. Jeon, and K. Kang, *Energy Environ. Sci.*, **7**, 538 (2014).
2. K. H. Choi, S. J. Cho, S. H. Kim, Y. H. Kwon, J. Y. Kim, and S. Y. Lee, *Adv. Funct. Mater.*, **24**, 44 (2014).
3. X. Ji and L. F. Nazar, *J. Mater. Chem.*, **10**, 9821 (2010).
4. Y. Wu, M. Gao, X. Li, Y. Liu, and H. Pan, *J. Alloys Compd.*, **608**, 220 (2014).
5. Y. Zhao, Y. Zhang, Z. Bakenova, and Z. Bakenov, *Front. Energy Res.*, **3**, 2 (2015).
6. L. Zeng, F. Pan, W. Li, Y. Jiang, X. Zhong, and Y. Yu, *Nanoscale*, **6**, 9579 (2014).
7. Q. Li, M. Liu, X. Qin, J. Wu, W. Han, G. Liang, D. Zhou, Y. B. He, B. Li, and F. Kang, *J. Mater. Chem. A*, **4**, 12973 (2016).
8. Y. Zhang, Y. Zhao, Z. Bakenov, A. Konarov, and P. Chen, *J. Power Sources*, **270**, 326 (2014).
9. F. Wu, J. Chen, L. Li, T. Zhao, and R. Chen, *J. Phys. Chem. C*, **115**, 24411 (2011).
10. G. C. Li, G. R. Li, S. H. Ye, and X. P. Gao, *Adv. Energy Mater.*, **2**, 1238 (2012).
11. C. Li, Y. Zou, J. Duan, Y. Wang, Z. Qi, and Z. Li, *Mater. Lett.*, **218**, 142 (2018).
12. Y. Wu, M. Gao, X. Li, Y. Liu, and H. Pan, *J. Alloys Compd.*, **608**, 220 (2014).
13. J. Li, K. Li, M. Li, D. Gosselink, Y. Zhang, and P. Chen, *J. Power Sources*, **252**, 107 (2014).
14. J. Ye, F. He, J. Nie, Y. Cao, H. Yang, and X. Ai, *J. Mater. Chem. A*, **3**, 7406 (2015).
15. H. Wang, Y. Yang, Y. Liang, J. T. Robinson, Y. Li, and A. Jackson, *Nano Lett.*, **11**, 2644 (2011).
16. C. Dillard, S. H. Chung, A. Singh, A. Manthiram, and V. Kalra, *Mater. Today Energy*, **9**, 336 (2018).
17. A. Mentbayeva, A. Belgibayeva, N. Umirov, Y. Zhang, I. Taniguchi, I. Kurmanbayeva, and Z. Bakenov, *Electrochim. Acta*, **217**, 242 (2016).
18. H. Peng, X. Wang, Y. Zhao, T. Tan, Z. Bakenov, and Y. Zhang, *Polymers (Basel).*, **10**, 399 (2018).
19. Q. Liu, J. Zhu, L. Zhang, and Y. Qiu, *Renew. Sustain. Energy Rev.*, **81**, 1825 (2018).
20. E. Baştürk, E. Çakmakçi, S. Madakbaş, and M. V. Kahraman, *Adv. Polym. Technol.*, **37**, 1774 (2017).
21. L. Huang, J. Cheng, G. Qu, X. Li, Y. Hu, W. Ni, D. Yuan, Y. Zhang, and B. Wang, *RSC Adv.*, **5**, 23749 (2015).
22. B. Oktay, E. Baştürk, M. V. Kahraman, and N. K. Apohan, *React. Funct. Polym.*, **127**, 10 (2018).
23. E. M. Eminoğlu and M. V. Kahraman, *Synth. Met.*, **183**, 29 (2013).
24. G. Sun, L. Sun, H. Xie, and J. Liu, *Nanomaterials*, **6**, 129 (2016).
25. V. Aravindan, J. Sundaramurthy, P. Suresh Kumar, Y.-S. Lee, S. Ramakrishna, and S. Madhavi, *Chem. Commun.*, **51**, 2225 (2015).
26. H. Peng, X. Wang, Y. Zhao, T. Tan, A. Mentbayeva, Z. Bakenov, and Y. Zhang, *J. Nanoparticle Res.*, **19**, 348 (2017).
27. T. Hara, A. Konarov, A. Mentbayeva, I. Kurmanbayeva, and Z. Bakenov, *Front. Energy Res.*, **3**, 22 (2015).
28. L. Ji, M. Rao, S. Aloni, L. Wang, E. J. Cairns, and Y. Zhang, *Energy Environ. Sci.*, **4**, 5053 (2011).
29. L. Huang, J. Cheng, G. Qu, X. Li, Y. Hu, and W. Ni, *RSC Adv.*, **5**, 23749 (2015).
30. D. Yang, W. Ni, J. Cheng, Z. Wang, T. Wang, Q. Guan, Y. Zhang, H. Wu, X. Li, and B. Wang, *Appl. Surf. Sci.*, **413**, 209 (2017).
31. H. Yao, G. Zheng, P. C. Hsu, D. Kong, J. J. Cha, W. Li, Z. W. Seh, M. T. McDowell, K. Yan, Z. Liang, V. K. Narasimhan, and Y. Cui, *Nat. Commun.*, **5**, 1 (2014).
32. T. N. L. Doan, M. Ghaznavi, Y. Zhao, Y. Zhang, A. Konarov, M. Sadhu, R. Tangirala, and P. Chen, *J. Power Sources*, **241**, 61 (2013).
33. J. Ye, F. He, J. Nie, Y. Cao, H. Yang, and X. Ai, *J. Mater. Chem. A*, **3**, 7406 (2015).
34. J. Wang, J. Yang, C. Wan, K. Du, J. Xie, and N. Xu, *Adv. Funct. Mater.*, **13**, 487 (2003).
35. A. Konarov, Z. Bakenov, H. Yashiro, Y. K. Sun, and S. T. Myung, *J. Power Sources*, **355**, 140 (2017).
36. F. Yin, X. Liu, Y. Zhang, Y. Zhao, A. Menbayeva, Z. Bakenov, and X. Wang, *Solid State Sci.*, **66**, 44 (2017).